AIAA JOURNAL
Vol. 47, No. 4, April 2009

Pressure, Temperature, and Velocity Measurements in Underexpanded Jets Using Laser-Induced Fluorescence Imaging

Sameer V. Naik,* Waruna D. Kulatilaka,† Krishna K. Venkatesan,‡ and Robert P. Lucht§
Purdue University, West Lafayette, Indiana 47907

DOI: 10.2514/1.37343

We report measurements of pressure, temperature, and velocity in an underexpanded jet using planar laser-induced fluorescence of nitric oxide. Ultraviolet transitions near 44, 097.5 cm^{-1} in the $A–X$ (0,0) system of nitric oxide were excited using narrow linewidth laser radiation generated from an optical parametric system, injection seeded using a distributed feedback diode laser. Planar laser-induced fluorescence images with excellent spatial resolution and signal-to-noise ratio were acquired by tuning the frequency of the laser radiation over the nitric oxide absorption line. The images were corrected on a shot-to-shot basis for fluctuations in the laser spatial profile. Line shapes constructed from the corrected planar laser-induced fluorescence images were used to determine pressure and temperature values along the centerline of the jet. Good agreement between laser-induced fluorescence and previously reported N_2 coherent anti-Stokes Raman scattering measurements was observed. The laser-induced fluorescence measurements also compared well with calculations of pressure and temperature using computational fluid dynamics codes. Velocity was measured in supersonic regions of the flowfield on the basis of the Doppler shift in the nitric oxide absorption lines. Planar laser-induced fluorescence images were acquired using laser sheets propagating at 90 and 45 degrees with respect to the flow direction; velocity was determined from the frequency shift of the absorption lines for these two shifts. The laser-induced fluorescence technique can potentially be applied to obtain instantaneous measurements of thermodynamic properties and multiple velocity components in high-speed turbulent flows.

I. Introduction

ANALYTICAL and numerical tools give great insight into the physics of supersonic and hypersonic flows. However, reliable measurements are essential to validate models and to implement design procedures with higher confidence. Laser-based diagnostic methods can provide the excellent spatial resolution and in situ measurement capabilities required to support computational fluid dynamics (CFD) calculations of supersonic and hypersonic flowfields. Such flowfields are challenging environments for the application of quantitative laser diagnostics.

Underexpanded jets, which provide test flowfields for high-speed compressible fluid flows, have been used extensively for laboratory measurements because well-characterized supersonic flowfields can be achieved with relatively inexpensive equipment. Adamson and Nicholls [1] presented the first comprehensive study regarding the structure of supersonic jets from highly underexpanded nozzles. Comparison of computed results with experimental photographs showed favorable agreement between jet boundary shape and Mach disc location at relatively low-pressure ratios. Recently, McDaniel et al. [2] reported a comprehensive comparison between experimental and numerical, as well as analytical/empirical, predictions for an underexpanded free jet. The work was specifically performed to provide a test medium for a hypersonic wind-tunnel facility designed to study rarefied flow phenomena.

Several research groups have developed advanced laser diagnostics for point and planar measurements of pressure, temperature, density, and velocity in compressible flows. Laser-induced fluorescence (LIF) of seeded iodine molecules excited via a sheet of single-mode, continuous wave (cw) argon-ion laser has been used for the measurement of velocity, based on determining the Doppler shift of the absorption line, in supersonic [3] and subsonic gas flows [4]. Over the last two decades, the laser-induced iodine fluorescence (LIIF) technique has evolved into a powerful method owing to the efforts of McDaniel et al. [5–8]. Fletcher and McDaniel [5] reported a two-line LIIF method, with excitation provided by tunable dye lasers, to measure temperatures in nonreacting supersonic flowfields. In a later development, the temperature dependence of broadband LIIF, excited using an argon-ion laser, was used to obtain spatially resolved planar temperature distributions [6]. The preceding broadband technique is especially attractive for measurements in highly three-dimensional, low-temperature compressible flows. The same research group also developed a novel approach to provide quantitative planar imaging of injectant mole-fraction distributions so as to evaluate three-dimensional mixing in compressible flows [7]. Hollo et al. [8] demonstrated the application of LIIF for planar velocity measurements in steady, symmetric flowfields. Fletcher and McDaniel [9], Hartfield et al. [10], Donohue and McDaniel [11,12] have applied the aforementioned LIIF techniques to conduct planar measurements of temperature, pressure, and velocity in a variety of flowfields, such as fuel injectors and nonreacting supersonic combustors.

Planar laser-induced fluorescence (PLIF) of nitric oxide (NO) has been used extensively to measure flow properties. Pulsed PLIF of a spectrally narrow absorption line of NO, excited using a broadband laser source, was implemented to image multiple velocity components in a highly underexpanded jet [13]. In later work, the same broadband technique was applied to obtain single-shot measurements of axial and radial velocity components in a free jet, generated using a shock tunnel [14]. McMillin et al. [15] reported a two-line NO-LIF technique to measure temperature using single-shot and frame-averaged spatially resolved images of a fuel jet in a heated supersonic crossflow. Danehy et al. [16] measured one

Presented as Paper 246 at the 46th AIAA Aerospace Sciences Meeting and Exhibit, Reno, Nevada, 7–10 January 2008; received 28 February 2008; revision received 10 October 2008; accepted for publication 10 October 2008. Copyright © 2008 by the American Institute of Aeronautics and Astronautics, Inc. All rights reserved. Copies of this paper may be made for personal or internal use, on condition that the copier pay the $10.00 per-copy fee to the Copyright Clearance Center, Inc., 222 Rosewood Drive, Danvers, MA 01923; include the code 0001-1452/09 $10.00 in correspondence with the CCC.

*Senior Research Associate, School of Mechanical Engineering, Room 90, Mechanical Engineering Building, 585 Purdue Mall; naiks@ecn.purdue.edu. AIAA Member (Corresponding Author).

†Currently Postdoctoral Research Associate, Combustion Research Facility, Sandia National Laboratories, Livermore, California. AIAA Member.

‡Currently Combustion Research Engineer, General Electric Global Research Center, Schenectady, New York. AIAA Member.

§Professor, School of Mechanical Engineering. AIAA Associate Fellow.

component of velocity in a Mach 7 hypersonic, separated flow around a cone; the uncertainty of measurements was about 100 m/s for velocities between −300 and 1300 m/s. Wilkes et al. [17] performed an experimental study of underexpanded axisymmetric nitrogen free jets seeded with NO with comparisons to CFD results. Jet structure data showed good agreement with numerical predictions; the qualitative comparison between experimental and computational images was reasonable.

In comparison to the preceding fluorescence-based approaches, filtered Rayleigh scattering (FRS) was developed to achieve suppression of background scattering so as to allow planar flowfield visualization and quantitative measurement of velocity, temperature, and density in unseeded high-speed gas flows [18]. Using the total intensity, Doppler shift, and spectral profile of the scattered light, density, velocity, and pressure, respectively, were determined. A theoretical model was developed for FRS and spatially resolved measurements of velocity, temperature, and pressure from time-averaged spectra were obtained in a supersonic free jet [19]. Frequency-modulated FRS techniques using Ti:Sapphire and solid-state diode lasers have been described for the simultaneous measurement of density and velocity at multiple locations in a gaseous flow using a single laser beam [20,21]. Planar Doppler velocimetry, using a molecular filter for simultaneous measurements of velocity and thermodynamic properties such as temperature and pressure, has been demonstrated as a powerful method for probing supersonic and hypersonic flows [22,23].

Nonlinear optical diagnostics offer an attractive alternative owing to the excellent resolution and elimination of background fluorescence, characterized by coherent Raman techniques. Stimulated Raman gain spectroscopy (SRGS) was applied for the measurement of velocity, based on the Doppler shift in the Q-branch spectra, in a subsonic N_2 jet from a converging nozzle [24]. In a following investigation, inverse Raman spectroscopy (IRS) was used to measure velocity, temperature, and density of nitrogen molecules in a supersonic flow generated inside a miniature wind tunnel [25]. The uncertainties of 5% for the velocity and 10% for the temperature and density measurements using IRS were considerably better compared to those for SRGS. Coherent anti-Stokes Raman scattering (CARS) measurement of velocity in a supersonic jet of methane agreed to within 4% of calculated value [26]. Woodmansee et al. [27] obtained high-resolution N_2 CARS spectra to acquire pressure, temperature, and density (using equation of state) measurements in supersonic flows based on the sensitivity of the rotational line structure of the N_2 vibrational Q-branch with respect to pressure and temperature. Excellent agreement between measurements and CFD computations was achieved along the centerline of an underexpanded jet.

Recently, we have performed PLIF imaging of nitric oxide in an underexpanded jet using a new type of tunable, pulsed optical parametric system that produces nearly transform-limited, narrow bandwidth laser radiation, similar to that described by Kulatilaka et al. [28]. We previously described the high-spectral-resolution NO-PLIF system, primarily demonstrating its capability for velocity measurement [29]. In this paper, we provide a detailed description of the experimental system and we report single-shot measurements of pressure, temperature, and velocity along the centerline of the underexpanded free jet. When using NO PLIF for velocity measurement, the laser linewidth $\Delta\nu_L$ was either much broader than the transition linewidth $\Delta\nu_T$ in the approach of Paul et al. [13] or comparable to $\Delta\nu_T$ in the technique described by Danehy et al. [16]. Hiller and Hanson [30] demonstrated simultaneous measurement of two velocity components and pressure using an approach similar to that described in this paper, that is, $\Delta\nu_L \ll \Delta\nu_T$; however, use of a single-frequency, high-power argon-ion laser along with iodine seeding was necessary to generate sufficient fluorescence intensity. Hartfield et al. [10] used a broadband laser for temperature measurement, whereas the pressure and velocity measurements were obtained by operating the same laser as a narrowband source.

In the current work, the linewidth of the laser used for excitation of NO is much narrower than the linewidth of the NO transition. High LIF signal levels are observed even in the low-temperature, low-pressure region of the flowfield. Although techniques similar to our approach have been described elsewhere [10,30], the current work demonstrates the capability of the narrow linewidth, tunable optical parametric system for simultaneous measurements of pressure, temperature, and velocity using pulses from a single laser system. The injection-seeding distributed feedback (DFB) diode laser can be scanned rapidly under computer control over the selected NO absorption transition; thus, the raw PLIF data are acquired rapidly and stored for data processing. These features motivate the further development of the optical parametric system to obtain instantaneous measurements of thermodynamic properties and velocity simultaneously in high-speed compressible flows.

II. Experiment

The experimental system was composed of three components, viz., the laser system to produce the ultraviolet (UV) radiation required for PLIF imaging, the flow system to generate the underexpanded supersonic jet, and the charge-coupled device (CCD) imaging camera and data acquisition system to collect and record the PLIF data. Figure 1 shows the details of an injection-seeded optical parametric system which produces nearly transform-limited laser radiation at 452 nm. An optical parametric oscillator (OPO) stage

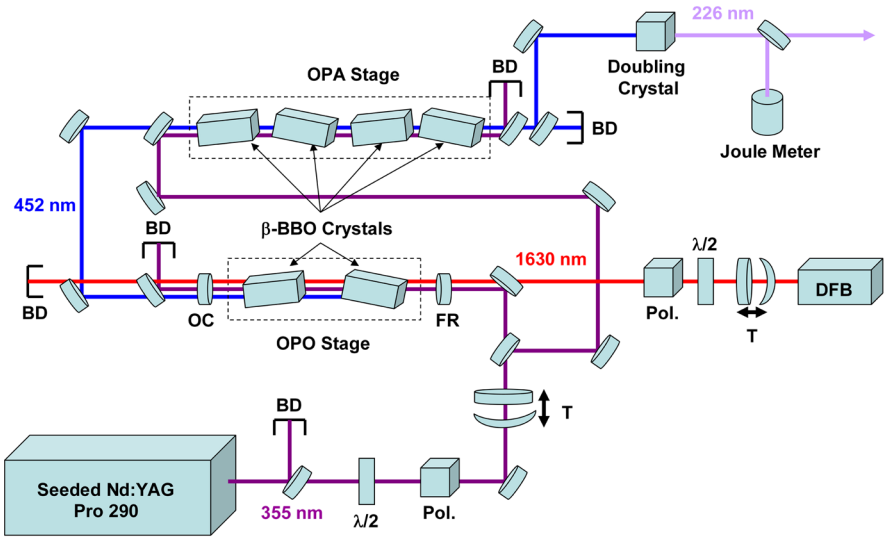

Fig. 1 Injection-seeded optical parametric oscillator/optical parametric amplifier (OPO/OPA) system to generate laser radiation near 226 nm for NO PLIF.

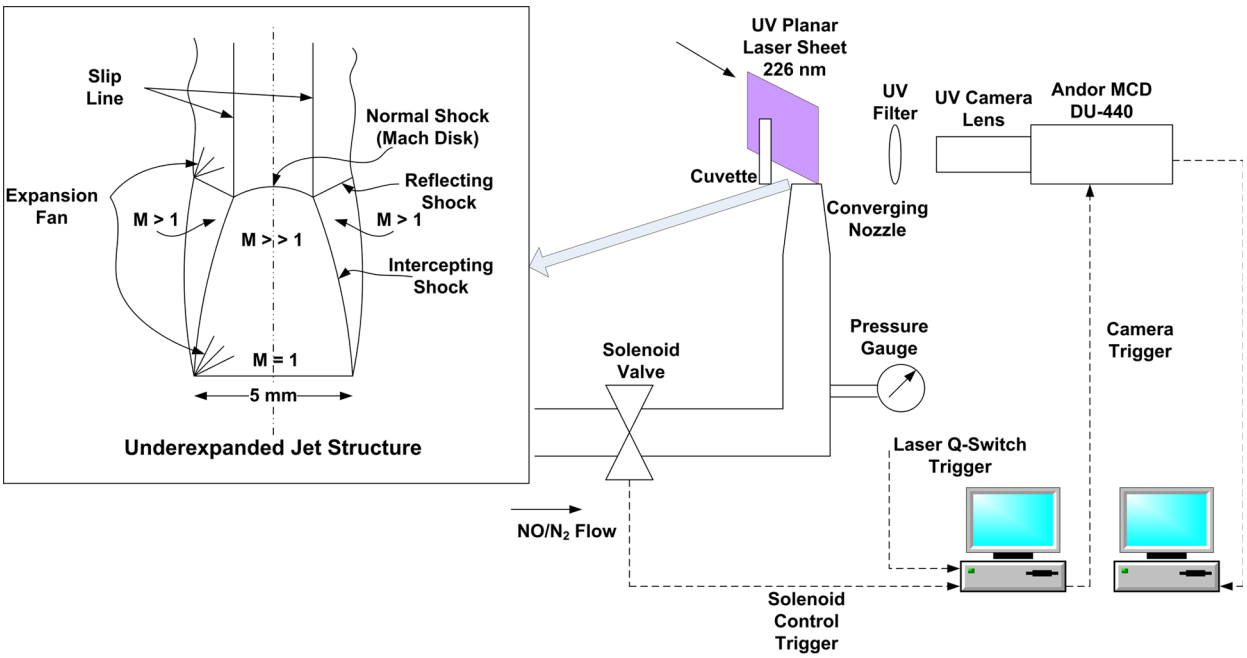

Fig. 2 Schematic of the flow, imaging, and data acquisition systems for NO PLIF.

was injection seeded at 1652 nm using a cw DFB diode laser. Two counter-rotating beta barium borate (β-BBO) crystals were pumped using $\sim$125 mJ/pulse of the third harmonic output (355 nm) of an injection-seeded Nd:YAG laser. The signal beam (452 nm) from the OPO stage was amplified using four counter-rotating β-BBO crystals, which were pumped by the third harmonic output of the same Nd:YAG laser, in an optical parametric amplifier (OPA) stage. The maximum signal beam energy at the output of the OPO/OPA system was approximately 20 mJ/pulse. The measured frequency bandwidth of the 452-nm signal beam was approximately 220 MHz full width at half-maximum [28]. This beam was then frequency-doubled using another β-BBO crystal in an Inrad Autotracker II to produce UV radiation at 226 nm for exciting the selected molecular transition in the A–X (0,0) electronic system of NO. The bandwidth of the 226-nm beam was not measured directly. It is estimated to be approximately 300 MHz by considering frequency doubling of a Gaussian spectrum. The maximum UV energy of 1.5 mJ/pulse was reduced to about 0.5 mJ/pulse using neutral density filters to prevent saturation of the NO transitions [13].

Figure 2 shows a schematic diagram of the experimental apparatus. A specially contoured convergent nozzle and solenoid valve were connected to high-pressure gas cylinders containing 300 ppm NO in buffer nitrogen. A pressure gauge was mounted upstream of the nozzle to record the stagnation pressure of the gas. At the nozzle exit, the flow of the high-pressure gas (NO seeded in N_2) produced a highly underexpanded jet after the solenoid valve was opened using a LabVIEW program. The stagnation pressure of the jet was approximately 5 atm. A sheet of UV light was formed using a combination of a cylindrical lens and a spherical lens. The sheet was focused in the horizontal dimension above the nozzle exit. The central portion of the laser sheet illuminated the underexpanded jet; the lateral dimension of the laser sheet was equal to the width of the jet. A quartz cuvette was filled with the 300 ppm NO in N_2 gas mixture at room temperature and pressure. The quartz cuvette was placed next to the nozzle exit such that an unintensified CCD camera (Andor MCD, DU-440) could image the flowfield and the cuvette in the same frame. The CCD array has 2048 pixels in the horizontal direction and 512 pixels in the vertical direction; the pixel size is 13.5 μm in each direction. The quantum efficiency of the CCD is approximately 25% near 226 nm. A UV camera lens along with a UV filter was used to collect the NO fluorescence signal. Figure 3 shows the timing sequence for synchronizing the solenoid valve and camera shutter opening with the laser pulses using a LabVIEW program. At a certain time, the solenoid valve in the NO/N_2 line was opened and the program triggered an AND gate 400 ms after opening the solenoid. The AND gate then triggered the CCD camera for the next one to three laser pulses, during which time fully developed images of the flowfield were recorded. The solenoid valve and the AND gate were switched off after capturing the images.

For our experiments, we scanned the temperature of the DFB seed laser of the OPO/OPA system so as to tune the resulting UV beam frequency over the $Q_{22}(5) + R_{12}(5)$ transition at 44, 097.53 cm^{-1} in the A–X (0,0) system of NO. The diode laser temperature was calibrated using a high-precision wave meter (HighFinesse Angstrom WS-6). While scanning the DFB, the angles of the β-BBO crystals in the OPO cavity and the OPA were unchanged. The seed laser was scanned over approximately 3 cm^{-1} and a PLIF image was obtained, using the procedure described previously, at 30 different UV frequencies to construct NO-LIF line shapes after carefully processing the raw images. The exposure time for the CCD was 90 ms; thus, the PLIF images were acquired nominally on a single-shot basis. We performed two different set of experiments: one in which the flow from the nozzle was perpendicular to the direction of laser sheet propagation (90 deg case) and the other for which the nozzle was tilted such that the flow from the nozzle

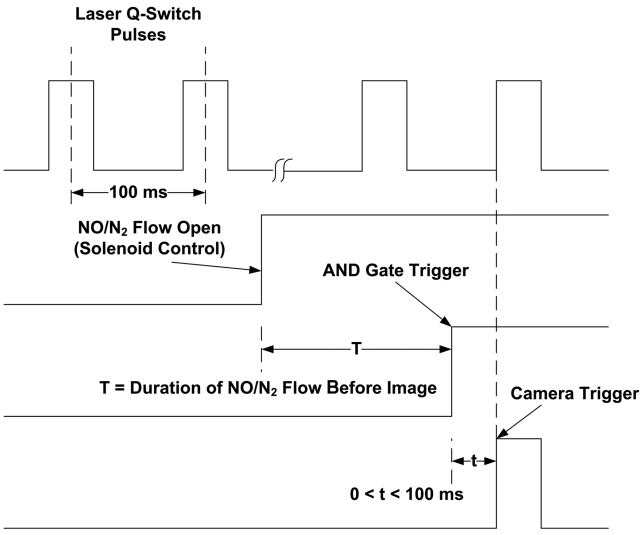

Fig. 3 Timing diagram for the NO-PLIF experiments.

intersected the laser sheet at 45 deg (45 deg case). The Doppler frequency shift between the 90 and 45 deg LIF line shapes was used to measure the velocity in the supersonic region upstream of the normal shock.

III. Image Processing

At each laser frequency, the one-dimensional spatial intensity distribution of the laser sheet orthogonal to the direction of propagation was obtained from fluorescence of NO in the cuvette. For a given laser shot, the flowfield and the cuvette were imaged in the same frame of the CCD, so that the raw images of the flowfield could be corrected by accounting for the shot-to-shot fluctuations in the laser spatial profile. A LabVIEW program was written for processing the raw images. For the 90 deg case, the vertical laser sheet propagated horizontally; therefore, a one-to-one mapping between the flowfield and cuvette images is sufficient. For the 45 deg case, the laser sheet was partially blocked using a knife edge and the exact angle was determined by reading pixel numbers along the sharp edge in the image. In this manner, a region of interest in the flowfield image could be accurately mapped to the corresponding region in the cuvette image. The total laser intensity for any axial location of interest in the flowfield was found by integrating in the corresponding region in the cuvette. The counts in the region of interest within the raw image of the flowfield were corrected by dividing with the laser intensity counts obtained from the corresponding region in the cuvette. It should be noted here that it is highly desirable to attain a uniform illumination of the region of interest so as to avoid such spatially dependent intensity corrections. Pfadler et al. [31] have demonstrated the advantage of using a microlens array beam homogenizer for planar laser measurements, in terms of measurement noise reduction and simplification of signal processing.

Figure 4 shows an experimental NO-LIF spectrum obtained via averaging over a chosen region of interest inside the cuvette for each laser frequency. Comparing the measured spectrum with a theoretical NO-LIF spectrum (calculated for 300 K and 1 atm), we note that a correction factor must be applied to the raw NO-LIF line shape obtained using the counts from the corrected flowfield images. The correction factor for each laser frequency was obtained by the division of the theoretical spectrum by the experimental NO-LIF spectrum shown in Fig. 4. The OPO/OPA signal output at 452 nm modulates as the DFB laser is scanned, primarily due to etalon effects in the OPO cavity. The correction factor is used to account for this nonreproducible variation in laser output during the scan. Because the variation of the OPO signal output changed with time, the spectral correction factor for each frequency was updated for each image. The preliminary NO-LIF line shapes were then multiplied with this correction factor to construct the line shapes shown in the remainder of this paper. The laser intensity normalization was implemented for each image with updated correction factors for each scan.

IV. Results and Discussion

Figure 5 shows typical PLIF images corrected for the spatial profile of the laser sheet at three different frequencies. For most images, the signal-to-noise ratio values were about 40:1 and 90:1 in the regions before and after the normal shock, respectively. These numbers are relatively high for the NO-PLIF approach with $\Delta\nu_L \ll \Delta\nu_T$; however, comparable results have previously been reported when seeding the flow with efficient fluorescing species, such as iodine or sodium, and by using long exposure times. The intercepting shock, normal shock, and reflecting shock are clearly seen in the images. Other features, such as the slip line and inner and outer shear layers downstream of the normal shock, are also visible. Furthermore, our investigation gives us the capability to extract high-spectral-resolution line shapes from these images to obtain accurate pressure, temperature, and velocity information simultaneously using single-shot images.

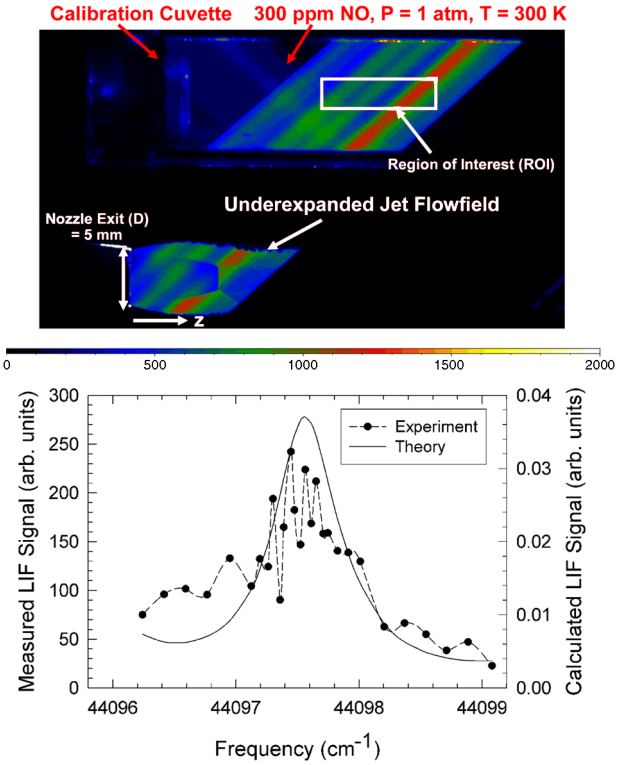

Fig. 4 Comparison between experimental and theoretical NO-LIF spectra from the calibration cuvette used to obtain the correction factor for flowfield images. A complete frame image showing the underexpanded jet and calibration cuvette is shown for reference. The modulation in the experimental NO-LIF signal from the selected region of interest in the cuvette is used to correct for the modulation of the signal beam energy from the OPO/OPA system.

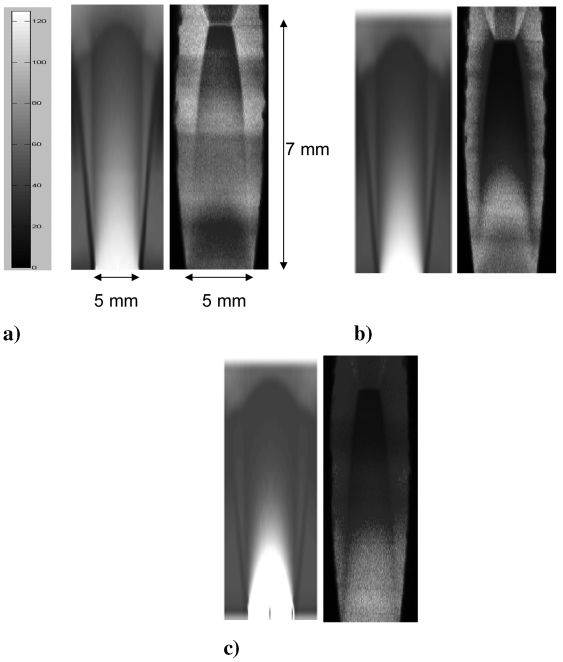

Fig. 5 Typical experimental NO-PLIF images (right panels) of the underexpanded supersonic jet flowfield at a) 44, 097.57 cm^{-1} ($\Delta\omega = 0$), b) 44, 097.98 cm^{-1} ($\Delta\omega = +0.41$ cm^{-1}), and c) 44, 099.05 cm^{-1} ($\Delta\omega = +1.48$ cm^{-1}). Calculated flowfield images (left panels) using FLUENT are shown for comparison at each DFB laser frequency. The images have been stretched in the axial direction.

In Fig. 5, the experimental PLIF image at three different DFB frequencies is compared with the corresponding image calculated using the results of FLUENT calculation of the underexpanded jet flowfield. A theoretical PLIF image was calculated assuming constant NO mole fraction throughout the flowfield of the underexpanded jet. For FLUENT calculations, the computational domain was axisymmetric and the size of the domain was large compared to the jet. The boundary conditions were set to pressure outlet everywhere except the axis of symmetry. An inviscid flow of nitrogen (ideal gas) was considered; the discretization was two-dimensional, explicit in space and one-dimensional, implicit in time. The pressure–velocity coupling was handled using the SIMPLE algorithm within FLUENT. An adaptive grid was necessary to resolve the various shock structures in the flowfield. The calculated pressure and temperature values along the jet centerline agree well with the more detailed Reynolds-averaged Navier Stokes simulation of the same flowfield [27]. There is a noticeable difference between the measured and computed shape of Mach disk. This discrepancy might arise from the fact that the turbulent interactions are not considered for our calculations. The physics of the fluid dynamics in the shear layer directly affect the shape and location of the Mach disk, owing to the coalescence of compression waves originating at the jet boundary. In the calculated PLIF images, nonzero LIF signals are shown outside the jet because the NO mole fraction was assumed to be constant throughout the flowfield.

One of the earliest studies of the underexpanded flowfield was reported by Bier and Schmidt [32]. Based on their results, the axial distance from the nozzle exit to the normal shock x_m and the diameter of the Mach disk D_m are given by

$$\frac{x_m}{D} = 0.67\left(\frac{p_0}{p_1}\right)^{1/2}; \qquad \frac{D_m}{x_m} = 0.42 \tag{1}$$

where D is the diameter of the nozzle and p_0/p_1 is the ratio of stagnation pressures across the nozzle. For our experimental conditions, we have $D = 5$ mm and $p_0/p_1 \cong 5$. Thus, $x_m = 7.5$ mm and $D_m = 3.1$ mm from Eq. (1). Based on the average of 10 PLIF images, the experimental values of x_m and D_m are found to be 7.3 and 2.3 mm, respectively. Thus, the observed axial location of the normal shock is within 3% of that predicted using Eq. (1), whereas the diameter of the Mach disk is approximately 20% lower.

Figure 6 displays the progression of NO-LIF line shapes along the centerline of the underexpanded jet. As the gas expands, the pressure and temperature decrease and the flow accelerates. At higher pressures near the nozzle exit, the LIF line is predominantly pressure broadened (Figs. 6a and 6b). The line narrows progressively along the jet centerline (Figs. 6c and 6d) and, right before the normal shock, the collisional linewidth is 0.18 cm^{-1} (Fig. 6e). Even in this region, the collisional linewidth is large compared to the Doppler linewidth. Right after the normal shock, the flow is recompressed, as evidenced from the broadened LIF line shape in Fig. 6f. For each axial position shown in Fig. 6, values for pressure and temperature obtained from LIF fits to experimental data are listed. These values are in good agreement with those previously measured using high-resolution N_2 CARS in an underexpanded supersonic jet using the same nozzle [27]. A direct comparison between the current data with those previously reported in the literature is presented later in the paper.

The LIF signal intensity can be written as

$$S_{\mathrm{LIF}} \propto f_B(T) N_{\mathrm{NO}} \frac{A}{A + Q(P,T)} \frac{1}{\Delta\omega_a\{1 + [2(\omega - \omega_a + \delta)/\Delta\omega_a]^2\}} \tag{2}$$

where $f_B(T)$ is the Boltzmann fraction, N_{NO} is the number density of NO (molecules/cm^3), A is the rate coefficient for spontaneous emission (s^{-1}), $Q(P,T)$ is the collisional quenching rate (s^{-1}), $\Delta\omega_a$ is the collisional linewidth (cm^{-1}), ω_a is the central frequency of NO transition, and δ is the frequency shift due to pressure (cm^{-1}). As discussed later, for the lowest pressure and temperature in the underexpanded jet right before the normal shock, the collisional linewidth is 0.18 cm^{-1}, whereas the Doppler linewidth is 0.06 cm^{-1}. The corresponding Voigt factor, $a = \sqrt{\ln 2}(\Delta\nu_C/\Delta\nu_D)$, has a value of 2.5. After recompression beyond the normal shock, the collisional linewidth is 0.8 cm^{-1}, whereas the Doppler linewidth is 0.09 cm^{-1}, and the corresponding value of the Voigt factor is 7.1. Therefore, Doppler broadening is not included in Eq. (2). We considered contributions from the $Q_{22}(5) + R_{12}(5)$, $R_{22}(2)$, and $P_{22}(12) + Q_{12}(12)$ transitions for our calculations. Pressure and temperature values along the jet centerline were obtained from FLUENT calculations. Collisional quenching rates were calculated using the theoretical pressure and temperature values and available quenching cross section data [33,34]. We considered quenching of the NO-LIF signal via collisions with NO and N_2. The empirical model of Settersten et al. [33] gives a cross section of $38.8°A^2$ at 300 K and $41.9°A^2$ at 100 K for NO–NO collisions; the average value was used in our calculations. The quenching cross section for NO–N_2 collisions is less $0.001°A^2$ at 300 K and negligibly small at 100 K [33]. Recent measurements of Settersten show little dependence of NO–N_2 quenching cross section down to 125 K.[¶] Therefore, a constant cross section with a rate coefficient scaling of $T^{-0.5}$ was assumed for these collisions. The exact frequencies and spontaneous emission coefficients for the relevant NO transitions were obtained from a comprehensive database for the NO A–X electronic system [35]. Collisional broadening and pressure shift coefficients were calculated using the best fit expressions for absorption line shape data measured in a shock tube [36]. The broadening and pressure shift coefficients (in cm^{-1}) can be written as $2\gamma = 0.583(295/T)^{0.75}P$ and $\delta = -0.18(295/T)^{0.56}P$, respectively, where T is temperature in Kelvin, and P is pressure in atm. We should note here that the preceding expressions were determined for the temperature range 295–2700 K. The extrapolation to temperatures down to 100 K may cause some systematic errors in pressure and temperature determination in the underexpanded jet.

In Fig. 7, we show the calculated LIF signal intensities and line shapes just downstream and just upstream of the normal shock for fixed pressure and varying temperature, as well as for fixed temperature and varying pressure conditions. Figure 7a shows that the LIF signal intensity depends on temperature in the region before the normal shock. However, the normalized line shapes shown in Fig. 7b essentially collapse to a single curve; thus, seeming to indicate that, for a given pressure, the LIF line shape is not very sensitive to temperature. The same trends are observed in the region after the normal shock, as seen in Figs. 7c and 7d, respectively. As seen in Fig. 7e, the LIF signal intensity also depends on pressure in the region before the normal shock. However, the normalized line shapes corresponding to different pressures clearly display frequency shifts for a given temperature, as shown in Fig. 7f. Similar trends are observed in the region after the normal shock, as observed from Figs. 7g and 7h. We observe that two neighboring NO transitions, viz., $P_{22}(12) + Q_{12}(12)$ at 44,095.70 cm^{-1} and $R_{22}(2)$ at 44,098.09 cm^{-1}, also influence the LIF line shapes. Additional information for determination of temperature and pressure is contained in the pressure shift of the central frequency of the line shape (Figs. 7f and 7h), as well as in the effect of the aforementioned secondary NO transitions that are close in frequency to the main spectral transition $Q_{22}(5) + R_{12}(5)$ at 44,097.57 cm^{-1}.

Based on the preceding observations, we can therefore fit the experimental NO-LIF line shapes, without knowing the precise value of temperature, to obtain the collisional linewidth. The collisional linewidth is proportional to $1/\sqrt{T}$; thus, we can obtain good approximation of the pressure using an initial guess value of temperature. The LIF line shapes were fit using a computer program described by Anderson et al. [37] to obtain pressure and temperature values. The computer program includes a detailed spectroscopic model for NO, and a Voigt profile is used for the line shape function. The collisional linewidth and temperature were the parameters that were varied to obtain the best fit to the experimental spectra. The fit

[¶]Settersten, T. B., Personal Communication, 2008.

values of pressure and temperature, when both collisional linewidth and temperature were free parameters, were indeed close to those predicted by CFD. For our experiments, we used initial guess values for temperature from FLUENT calculations for more accurate determination of pressure. In practical flowfields, however, such guess values from predictions may not be available. Therefore, we performed a sensitivity study in which the initial temperature guess was varied from 50 to 300 K. The corresponding change in the pressure value (or the collisional linewidth) was approximately $\pm 25\%$ of the nominal value reported in Fig. 6. The updated value of pressure was then used to determine the temperature. The resulting temperature values were found to be within ± 30 K of the initial guess at most locations. In the low-temperature region of the flowfield, the error bars are relatively larger, whereas the preceding method gives temperature values within 15% of predicted values above 200 K. More accurate temperature values can presumably be obtained using the ratio of LIF signal intensities from two transitions; however, in the current experiment, we scanned the DFB completely over only one major spectral feature of NO. However, as discussed previously, neighboring rotational transitions of NO influence the line shape of the major spectral feature.

In Fig. 8, we compare the pressure and temperature values measured using NO LIF with previously reported N_2 CARS measurements and CFD calculations. Clearly, the LIF and CARS measurements are in excellent agreement with one another and computations, except that predicted values are somewhat lower compared with data in the region downstream of the normal shock. The calculated pressure and temperature ratios using isentropic relationships are 10.33 and 2.68, respectively, across the normal shock. The pressure and temperature ratios determined from the

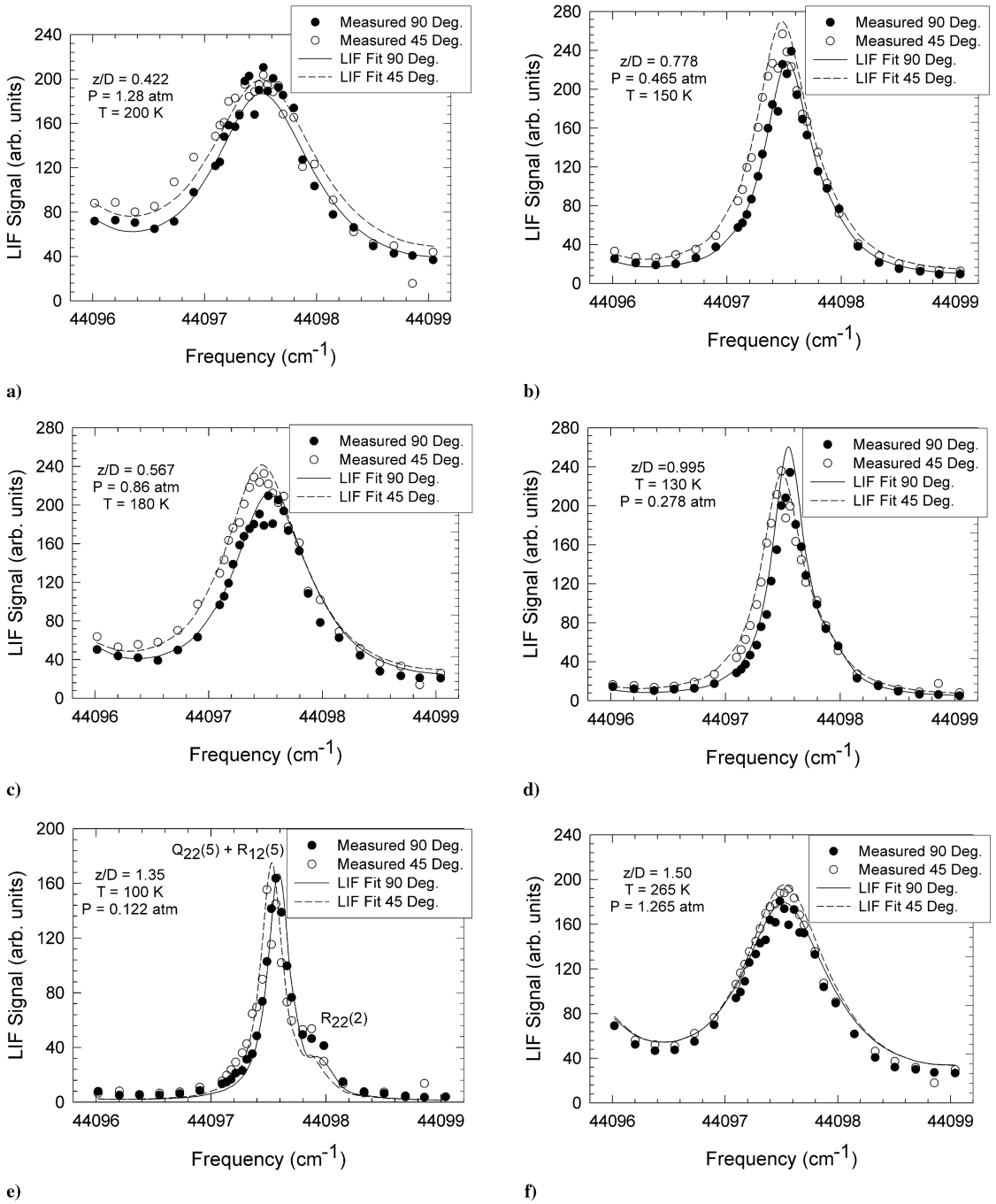

Fig. 6 Measured NO-LIF line shapes at six different axial locations along the centerline of the underexpanded jet. Pressure and temperature values from theoretical fits to the experimental LIF line shapes are shown for each location.

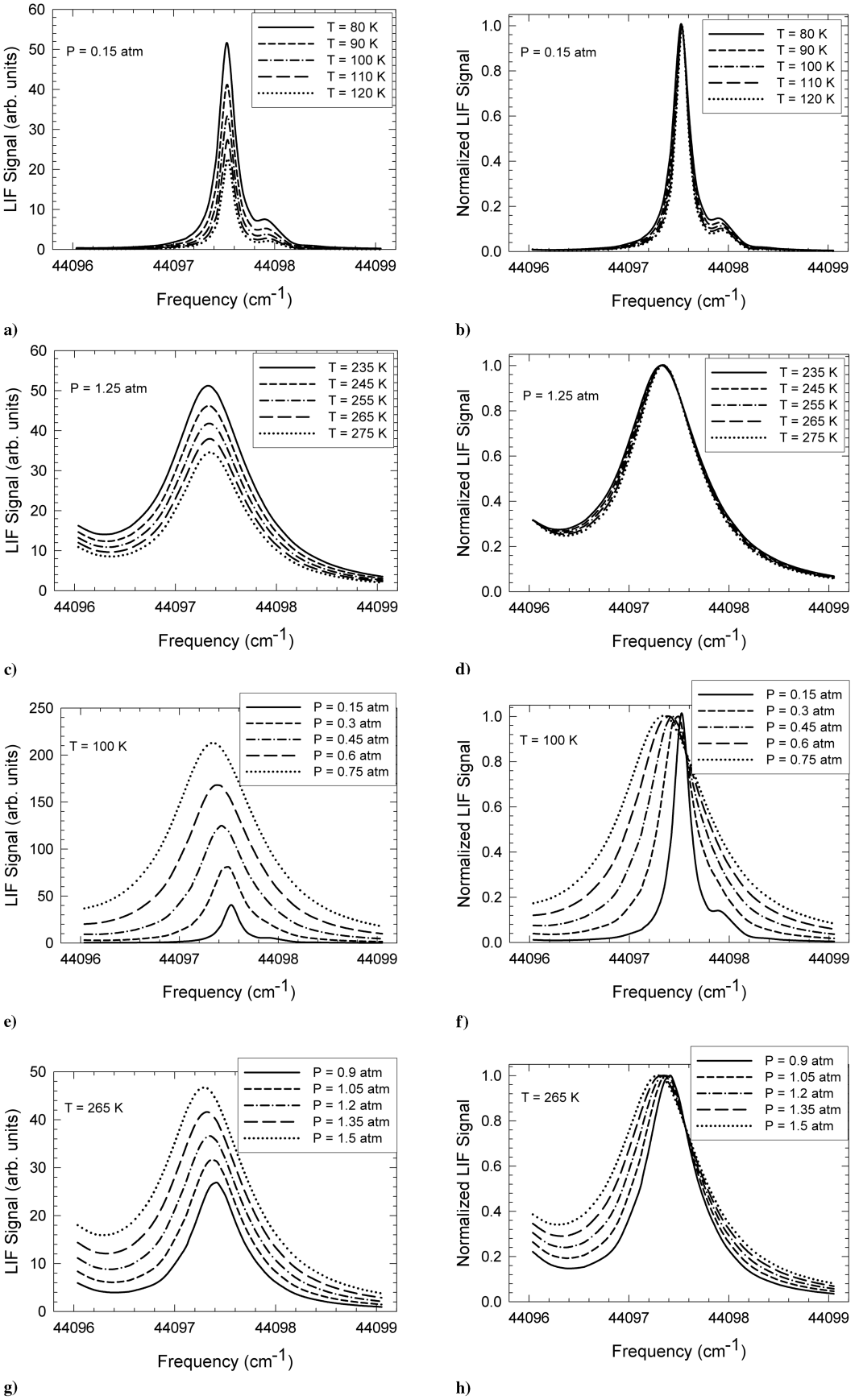

Fig. 7 Calculated LIF signal intensity variations with temperature for a given pressure, and with pressure for a given temperature, before and after the normal shock in the underexpanded jet.

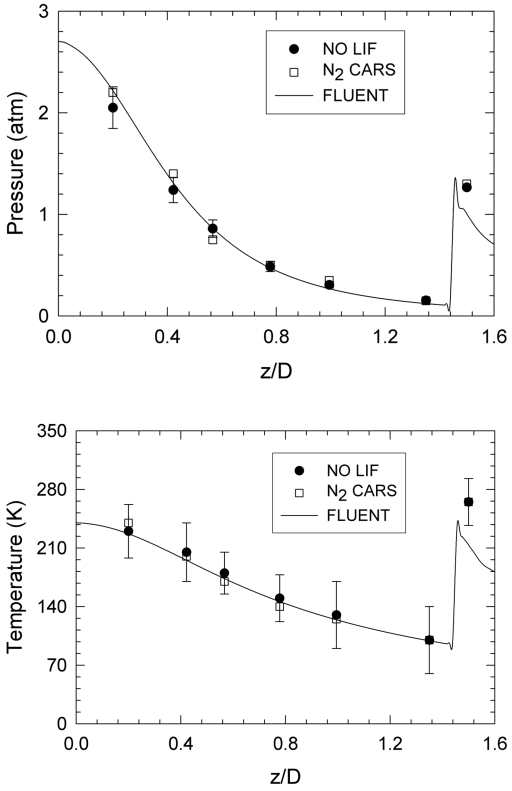

Fig. 8 Comparison between measured and computed pressure and temperature along the jet centerline.

PLIF images are 10.36 and 2.65, respectively. These experimental values compare very well with those calculations. Because the collisional linewidth was determined accurately, we have used conservative error bars of 10% for the pressure measurement. The error bars on temperature values were obtained using the sensitivity analysis described earlier. We should also note here that the LIF measurements are extracted from NO-PLIF images acquired using single laser shots, whereas the CARS data are averaged using 100 single-shot N_2 spectra. The LIF technique offers not only experimental simplicity but also good sensitivity and the capability for extracting accurate thermodynamic information.

Figure 9 displays the variation of the LIF signal along the jet centerline for different frequencies above and below the center transition frequency; experimental LIF signals are compared with theoretical LIF intensities calculated using FLUENT results and Eq. (2). The experimental data were scaled so as to best match calculated signal levels near the normal shock. The numerical grid near the Mach disk location was refined so as to resolve the shock structures sufficiently. However, an artificial spike downstream of the normal shock is observed in the calculated temperature and pressure field; the corresponding feature is also seen in the theoretical LIF signal intensity profiles in Fig. 9. The theoretical and experimental profiles are in good agreement for regions in the vicinity of the normal shock ($z/D \geq 0.6$) at all frequencies. However, for all excitation wavelengths, the experimental LIF signal at the nozzle exit is low when compared with the calculated LIF intensity by a factor of 2. The raw images indicate neither absorption of the laser sheet nor saturation of the CCD detector. For the $Q_{22}(5) + R_{12}(5)$ transition, over a 5-mm path length through 300 ppm NO in N_2, the peak absorption at the nozzle exit condition ($T = 240$ K, $P = 2.7$ atm) is calculated to be $\sim$1.5% using LIFSIM [38]. Therefore, laser sheet absorption or radiative trapping cannot explain the low signal levels near the nozzle exit. Vignetting effects related to the imaging optics were not considered. Furthermore, the selection of region of interest in the calibration cuvette could affect the value of correction factor. In future work, we will investigate the aforementioned issues regarding the calibration cuvette and vignetting.

For our experimental conditions, we have previously reported that the measured velocity of 500 ± 100 m/s at $z/D = 1.35$ is in good agreement with isentropic calculations [29]. The measured Doppler shift is 0.05 ± 0.01 cm^{-1} which corresponds to a Mach number of 2.5 ± 0.5 just upstream of the normal shock. Figure 10 shows the comparison between measured and calculated velocity profile along the jet centerline. In the supersonic region before the normal shock, the computed velocity and temperature values are 625 m/s and 95 K, respectively; the corresponding Mach number of 3.2 compares reasonably well with that obtained from the measured velocity. The measured velocity is within 20% of that calculated using FLUENT at all locations. The agreement between measured and calculated velocities deteriorates closer to nozzle, as expected due to the decreasing frequency shift. The measured Doppler shift values are low for our experimental configuration, with the highest being 0.05 cm^{-1}. The large uncertainty of 100 m/s in the velocity measurement corresponds to a Doppler shift of 0.01 cm^{-1}, the minimum value of which is limited by the resolution of the wave meter used to measure the wavelength of the 452 nm laser beam and by the temperature tuning capability of the DFB laser. In addition to the estimated random error of 0.01 cm^{-1} in the determination of the Doppler shift for each pair of 90 and 45 deg spectra, there is a possibility of a systematic error due to drift in the absolute wave meter reading from day-to-day. The 90 and 45 deg images were acquired on different days. This may account for the low values of the experimental velocity compared to that computed using CFD. Potential systematic errors due to the wave meter reading drift will be eliminated in future experiments by acquiring the 90 and 45 deg images simultaneously.

Pulse-burst lasers produce high energy pulses (10–100 mJ/pulse) at repetition rates in excess of 10 MHz [39,40] and have been applied for imaging applications in high-speed gas flows [41,42]. A pulse-burst laser could be combined with our optical parametric system along with pulse dye amplifiers (PDA), if required, so as to perform instantaneous measurements using high-speed framing cameras. Indeed, Jiang et al. [43] have recently demonstrated the ability to generate ultra-high-frequency sequences of tunable, high-intensity laser pulses using an OPO pumped by the third harmonic output of a Nd:YAG laser. In future work, we plan to employ such a laser system to obtain velocity, pressure, and temperature using NO PLIF at high frame rates in supersonic flows. In the near term, we will demonstrate the application of an OPO/PDA system for measurements inside a supersonic flow facility. Instantaneous measurements of pressure, temperature, and velocity could also be performed using multiple laser and camera systems. PLIF images using two or three different excitation frequencies could be acquired with time delays on the order of 100 ns between exposures by using multiple Nd:YAG/OPO systems and fast framing cameras. Such measurements will be very useful for the study of transport phenomena and turbulence effects in high-speed gas flows.

V. Conclusions

We have performed planar LIF of NO in a highly underexpanded supersonic jet for simultaneous measurements of velocity, pressure, and temperature. We acquired PLIF images with high spatial resolution and excellent signal-to-noise ratios using narrow linewidth laser radiation generated from an injection-seeded optical parametric system. The PLIF images were corrected for intensity variations in the spatial profile of the laser beam and images acquired for different excitation frequencies were used to construct spectral line shapes. Pressure and temperature were obtained by fitting the collisionally broadened NO line shapes. Measured values of pressure and temperature were found to be in very good agreement with previously reported high-resolution N_2 CARS measurements. The measured profiles of pressure, temperature, and velocity were also compared with CFD computations, and, in general, agreement between experiment and theory was satisfactory. The potential of the

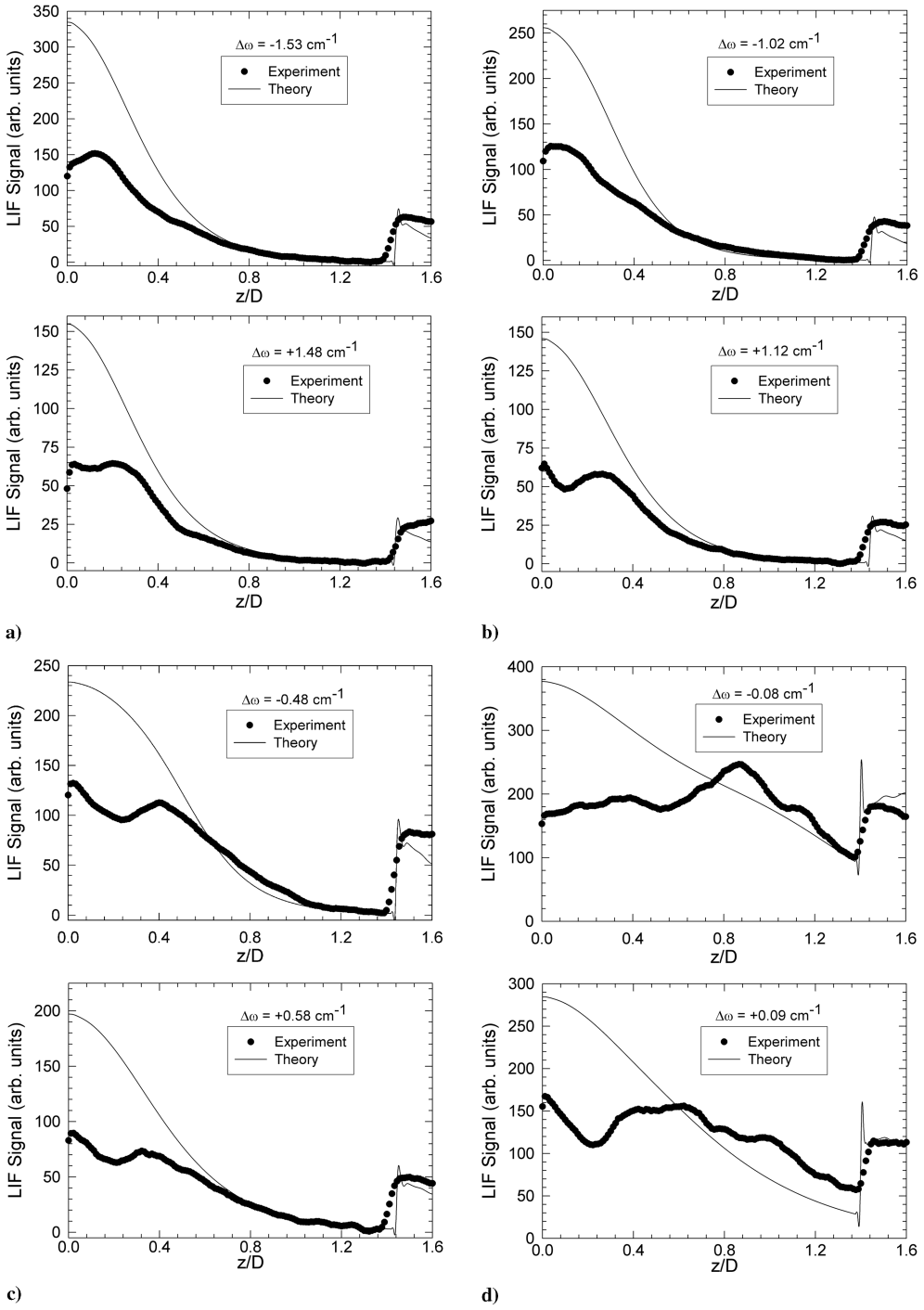

Fig. 9 Comparison between measured and calculated LIF signal along the jet centerline for different laser frequencies.

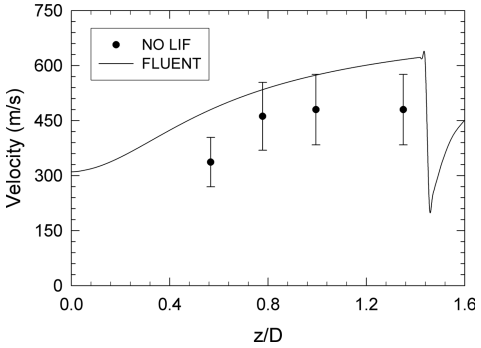

Fig. 10 Comparison between measured and computed velocity along the jet centerline.

LIF technique for velocity measurements in hypersonic flows and extension of the optical parametric system to perform instantaneous imaging of velocity and thermodynamic properties was discussed.

Acknowledgment

Funding for this research was provided by the U.S. Air Force Office of Scientific Research under Contract No. FA9550-04-1-0425 (John Schmisseur, Program Manager).

References

[1] Adamson, T. C., and Nicholls, J. A., "On the Structure of Jets from Highly Underexpanded Nozzles into Still Air," *Journal of the Aero/Space Sciences*, Vol. 26, No. 1, Jan. 1959, pp. 16–24.

[2] McDaniel, J. C., Glass, C. E., Staack, D., and Miller, C. G., "Experimental and Computational Comparison of an Underexpanded Jet Flowfield," AIAA Paper 2002-0305, Jan. 2002.
[3] McDaniel, J. C., Hiller, B., and Hanson, R. K., "Simultaneous Multiple-Point Velocity Measurements Using Laser-Induced Iodine Fluorescence," *Optics Letters*, Vol. 8, No. 1, 1983, pp. 51–53.
[4] Hiller, B., McDaniel, J. C., Rea, E. C., Jr., and Hanson, R. K., "Laser-Induced Fluorescence Technique for Velocity Field Measurements in Subsonic Gas Flows," *Optics Letters*, Vol. 8, No. 9, 1983, pp. 474–476.
[5] Fletcher, D. G., and McDaniel, J. C., "Temperature Measurement in a Compressible Flow Field Using Laser-Induced Iodine Fluorescence," *Optics Letters*, Vol. 12, No. 1, 1987, pp. 16–18.
[6] Hartfield, R. J., Jr., Hollo, S. D., and McDaniel, J. C., "Planar Temperature Measurement in Compressible Flows Using Laser-Induced Iodine Fluorescence," *Optics Letters*, Vol. 16, No. 2, 1991, pp. 106–108.
[7] Hartfield, R. J., Jr., Abbitt, J. D., III, and McDaniel, J. C., "Injectant Mole-Fraction Imaging in Compressible Mixing Flows Using Planar Laser-Induced Iodine Fluorescence," *Optics Letters*, Vol. 14, No. 16, 1989, pp. 850–852.
[8] Hollo, S. D., Hartfield, R. J., Jr., and McDaniel, J. C., "Planar Velocity Measurement in Symmetric Flow Fields with Laser-Induced Iodine Fluorescence," *Optics Letters*, Vol. 19, No. 3, 1994, pp. 216–218.
[9] Fletcher, D. G., and McDaniel, J. C., "Laser-Induced Iodine Fluorescence Technique for Quantitative Measurement in a Non-reacting Supersonic Combustor," *AIAA Journal*, Vol. 27, No. 5, 1989, pp. 575–580.
doi:10.2514/3.10148
[10] Hartfield, R. J., Jr., Hollo, S. D., and McDaniel, J. C., "Planar Measurement Technique for Compressible Flows Using Laser-Induced Iodine Fluorescence," *AIAA Journal*, Vol. 31, No. 3, 1993, pp. 483–490.
doi:10.2514/3.11355
[11] Donohue, J. M., and McDaniel, J. C., "Complete Three-Dimensional Multiparameter Mapping of a Supersonic Ramp Fuel Injector Flowfield," *AIAA Journal*, Vol. 34, No. 3, 1996, pp. 455–462.
doi:10.2514/3.13089
[12] Donohue, J. M., and McDaniel, J. C., "Computer-Controlled Multiparameter Flowfield Measurements Using Planar Laser-Induced Iodine Fluorescence," *AIAA Journal*, Vol. 34, No. 8, 1996, pp. 1604–1611.
doi:10.2514/3.13278
[13] Paul, P. H., Lee, M. P., and Hanson, R. K., "Molecular Velocity Imaging of Supersonic Flows Using Pulsed Planar Laser-Induced Fluorescence of NO," *Optics Letters*, Vol. 14, No. 9, 1988, pp. 417–419.
[14] Palmer, J. L., and Hanson, R. K., "Single-Shot Velocimetry Using Planar Laser-Induced Fluorescence Imaging of Nitric Oxide," AIAA Paper 1993-2020, June 1993.
[15] McMillin, B. K., Palmer, J. L., and Hanson, R. K., "Temporally Resolved, Two-Line Fluorescence Imaging of NO Temperature in a Transverse Jet in a Supersonic Cross Flow," *Applied Optics*, Vol. 32, No. 36, 1993, pp. 7532–7545.
[16] Danehy, P. M., Mere, P., Gaston, M. J., O'Byrne, S., Palma, P. C., and Houwing, A. F. P., "Fluorescence Velocimetry of the Hypersonic, Separated Flow over a Cone," *AIAA Journal*, Vol. 39, No. 7, 2001, pp. 1320–1328.
doi:10.2514/2.1450
[17] Wilkes, J. A., Glass, C. E., Danehy, P. M., and Nowak, R. J., "Fluorescence Imaging of Underexpanded Jets and Comparison with CFD," AIAA Paper 2006-910, Jan. 2006.
[18] Miles, R. B., and Lempert, W. R., "Two Dimensional Measurement of Density, Velocity, and Temperature in Turbulent High Speed Air Flows by UV Rayleigh Scattering," *Applied Physics B, Photophysics and Laser Chemistry*, Vol. 51, No. 1, 1990, pp. 1–7.
doi:10.1007/BF00332317
[19] Forkey, J. N., Finkelstein, N. D., Lempert, W. R., and Miles, R. B., "Demonstration and Characterization of Filtered Rayleigh Scattering for Planar Velocity Measurements," *AIAA Journal*, Vol. 34, No. 3, 1996, pp. 442–448.
doi:10.2514/3.13087
[20] Grinstead, J. H., Finkelstein, N. D., and Lempert, W. R., "Doppler Velocimetry in a Supersonic Jet by Use of Frequency-Modulated Filtered Light Scattering," *Optics Letters*, Vol. 22, No. 5, 1997, pp. 331–333.
doi:10.1364/OL.22.000331
[21] Mach, J., and Varghese, P. L., "Velocity Measurements by Modulated Filtered Rayleigh Scattering Using Diode Lasers," *AIAA Journal*, Vol. 37, No. 6, 1999, pp. 695–699.
doi:10.2514/2.797
[22] Elliott, G. S., Samimy, M., and Arnette, S., "A Molecular Filter Based Velocimetry Technique for High Speed Flows," *Experiments in Fluids*, Vol. 18, Nos. 1–2, 1994, pp. 107–118.
doi:10.1007/BF00209367
[23] Clancy, P. S., Samimy, M., and Erskine, W. R., "Planar Doppler Velocimetry: Three-Component Velocimetry in Supersonic Jets," *AIAA Journal*, Vol. 37, No. 6, 1999, pp. 700–707.
doi:10.2514/2.798
[24] Herring, G. C., Fairbank, W. M., Jr., and She, C. Y., "Observation and Measurement of Molecular Flow Using Stimulated Raman Gain Spectroscopy," *IEEE Journal of Quantum Electronics*, Vol. 17, No. 10, 1981, pp. 1975–1976.
doi:10.1109/JQE.1981.1070647
[25] Herring, G. C., Lee, S. A., and She, C. Y., "Measurements of a Supersonic Velocity in a Nitrogen Flow Using Inverse Raman Spectroscopy," *Optics Letters*, Vol. 8, No. 4, 1983, pp. 214–216.
[26] Gustafson, E. K., McDaniel, J. C., and Byer, R. L., "CARS Measurement of Velocity in a Supersonic Jet," *IEEE Journal of Quantum Electronics*, Vol. 17, No. 12, 1981, pp. 2258–2259.
doi:10.1109/JQE.1981.1070736
[27] Woodmansee, M. A., Lucht, R. P., and Dutton, J. C., "Development of High-Resolution N_2 Coherent Anti-Stokes Raman Scattering for Measuring Pressure, Temperature, and Density in High-Speed Gas Flows," *Applied Optics*, Vol. 39, No. 33, 2000, pp. 6243–6256.
doi:10.1364/AO.39.006243
[28] Kulatilaka, W. D., Anderson, T. N., Bougher, T. L., and Lucht, R. P., "Development of Injection-Seeded, Pulsed Optical Parametric Generator/Oscillator Systems for High-Resolution Spectroscopy," *Applied Physics B, Photophysics and Laser Chemistry*, Vol. 80, No. 6, 2005, pp. 669–680.
doi:10.1007/s00340-005-1772-y
[29] Kulatilaka, W. D., Naik, S. V., and Lucht, R. P., "Development of High-Spectral-Resolution Planar Laser-Induced Fluorescence Imaging Diagnostics for High-Speed Gas Flows," *AIAA Journal*, Vol. 46, No. 1, 2008, pp. 17–20.
doi:10.2514/1.34971
[30] Hiller, B., and Hanson, R. K., "Simultaneous Planar Measurements of Velocity and Pressure Fields in Gas Flows Using Laser-Induced Fluorescence," *Applied Optics*, Vol. 27, No. 1, 1988, pp. 33–48.
[31] Pfadler, S., Beyrau, F., Löffler, M., and Leipertz, A., "Application of a Beam Homogenizer to Planar Laser Diagnostics," *Optics Express*, Vol. 14, No. 22, 2006, pp. 10171–10180.
doi:10.1364/OE.14.010171
[32] Bier, K., and Schmidt, B., "Shape of a Compression Shock in Free Expanding Gas Jet," *Zeitschrift für Angewandte Physik*, Vol. 13, 1961, pp. 493–500.
[33] Settersten, T. B., Patterson, B. D., and Gray, J. A., "Temperature- and Species-Dependent Quenching of NO $A^2\Sigma^+$ ($v' = 0$) Probed by Two-Photon Laser-Induced Fluorescence Using a Picosecond Laser," *Journal of Chemical Physics*, Vol. 124, No. 23, 2006, pp. 234308.1–234308-14.
doi:10.1063/1.2206783
[34] Settersten, T. B., Patterson, B. D., Kronemayer, H., Sick, V., Schulz, C., and Daily, J. W., "Branching Ratios for Quenching of Nitric Oxide $A^2\Sigma^+$ ($v' = 0$) to $X^2\Pi$ ($v'' = 0$)," *Physical Chemistry Chemical Physics*, Vol. 8, No. 45, 2006, pp. 5328–5338.
doi:10.1039/b608619e
[35] Reisel, J. R., Carter, C. D., and Laurendeau, N. M., "Einstein Coefficients for Rotational Lines of the (0,0) Band of the NO $A^2\Sigma^+ - X^2\Pi$ System," *Journal of Quantitative Spectroscopy and Radiative Transfer*, Vol. 47, No. 1, 1992, pp. 43–54.
doi:10.1016/0022-4073(92)90078-I
[36] Chang, A. Y., DiRosa, M. D., and Hanson, R. K., "Temperature Dependence of Collision Broadening and Shift in the NO A-X (0,0) Band in the Presence of Argon and Nitrogen," *Journal of Quantitative Spectroscopy and Radiative Transfer*, Vol. 47, No. 5, 1992, pp. 375–390.
doi:10.1016/0022-4073(92)90039-7
[37] Anderson, T. N., Lucht, R. P., Barron-Jimenez, R., Hanna, S. F., Caton, J. A., Walther, T., Roy, S., Brown, M. S., Gord, J. R., Critchley, I., and Flamand, L., "Combustion Exhaust Measurements of Nitric Oxide with an Ultraviolet Diode-Laser-Based Absorption Sensor," *Applied Optics*, Vol. 44, No. 8, 2005, pp. 1491–1502.
doi:10.1364/AO.44.001491
[38] Bessler, W. G., Schulz, C., Sick, V., and Daily, J. W., "A Versatile Modeling Tool for Nitric Oxide LIF Spectra," *Proceedings of the Third Joint Meeting of the U.S. Sections of the Combustion Institute*, Paper PI05, March 2003.

[39] Wu, P. P., and Miles, R. B., "High-Energy Pulse-Burst Laser System for Megahertz-Rate Flow Visualization," *Optics Letters*, Vol. 25, No. 22, 2000, pp. 1639–1641. doi:10.1364/OL.25.001639

[40] Thurow, B., Jiang, N., Samimy, M., and Lempert, W., "Narrow-Linewidth Megahertz-Rate Pulse-Burst Laser for High-Speed Flow Diagnostics," *Applied Optics*, Vol. 43, No. 26, 2004, pp. 5064–5073. doi:10.1364/AO.43.005064

[41] Wu, P., Lempert, W. R., and Miles, R. B., "Megahertz Pulse-Burst Laser and Visualization of Shock-Wave/Boundary-Layer Interaction," *AIAA Journal*, Vol. 38, No. 4, 2000, pp. 672–679. doi:10.2514/2.1009

[42] Thurow, B. S., Jiang, N., Lempert, W. R., and Samimy, M., "Development of Megahertz-Rate Planar Doppler Velocimetry for High-Speed Flows," *AIAA Journal*, Vol. 43, No. 3, 2005, pp. 500–511. doi:10.2514/1.7749

[43] Jiang, N., Lempert, W. R., Switzer, G. L., Meyer, T. R., and Gord, J. R., "Narrow-Linewidth Megahertz-Repetition-Rate Optical Parametric Oscillator for High-Speed Flow and Combustion Diagnostics," *Applied Optics*, Vol. 47, No. 1, 2008, pp. 64–71. doi:10.1364/AO.47.000064

N. Clemens
Associate Editor